

Supporting Information for

**KCoO₂-Type Layered Nitrides Ca_{1-x}Eu_xTiN₂: Structural Stability,
Electrical Properties and Eu Coordination Chemistry**

Junwei Liu¹, Bowen Zhang¹, Shenglin Lu¹, Xing Ming^{*,1,2}, Xiaojun Kuang^{*,1,3}

1. *MOE Key Laboratory of New Processing Technology for Nonferrous Metals and Materials, Guangxi Key Laboratory of Optical and Electronic Materials and Devices, College of Materials Science and Engineering, Guilin University of Technology, Guilin 541004, P. R. China*
2. *College of Science, Guilin University of Technology, Guilin 541004, P. R. China*
3. *Guangxi Key Laboratory of Electrochemical and Magnetochemical Functional Materials, College of Chemistry and Bioengineering, Guilin University of Technology, Guilin 541006, P. R. China*

* E-mail: mingxing@glut.edu.cn (X.M.); kuangxj@glut.edu.cn (X.K.)

Table S1. Changes in unit cell parameters of $\text{Ca}_{1-x}\text{Eu}_x\text{TiN}_2$ solid solution.

x	a (Å)	b (Å)	c (Å)	V (Å ³)	b/a ratio
0	3.9365	3.6131	7.5421	107.3	0.91785
0.05	3.9344(1)	3.6280(1)	7.5501(2)	107.774(7)	0.92212
0.10	3.9314(1)	3.6423(1)	7.5544(2)	108.178(7)	0.92646
0.15	3.9274(2)	3.6558(2)	7.5574(3)	108.51(1)	0.93084
0.20	3.9245(2)	3.6666(2)	7.5600(3)	108.78(1)	0.93428
0.25	3.9134(2)	3.6946(3)	7.5647(4)	109.37(1)	0.94409
0.30	3.9097(4)	3.7061(4)	7.5679(8)	109.61(2)	0.94792
0.35	3.9047(4)	3.7164(5)	7.5701(9)	109.85(2)	0.95178
0.40	3.9050(4)	3.7162(4)	7.5685(8)	109.83(2)	0.95165

Table S2. Theoretically calculated bond lengths and bond angles of the orthorhombic and tetragonal phases EuTiN₂ within different magnetic structures.

Orthorhombic				
FM	Eu-N1 (Å)	Eu-N2 (Å)	Ti-N1 (Å)	Ti-N2 (Å)
	3.325×2	2.730×4	2.042×2	1.856
	3.122×2	2.502	2.040×2	
N1-Eu-N1 (°)		N2-Eu-N2(°)	N1-Eu-N2 (°)	
	50.110×4	91.413×4	63.856×4	63.571×4
	74.709	92.051×2	143.784×2	113.909×4
	72.431	$87.880 \times 2 / 180 \times 2$	142.645×2	113.667×4
N1-Ti-N2 (°)		Eu-N1-Ti (°)	Eu-N2-Ti (°)	N1-Ti-N1(°)
	105.849×2	69.633×2	180	84.172×4
	111.828×2	74.473×2		$136.344 / 148.302$
AFM	Eu-N1 (Å)	Eu-N2 (Å)	Ti-N1 (Å)	Ti-N2 (Å)
	3.171×2	2.732×4	2.041×2	1.855
	3.264×2	2.502	2.040×2	
N1-Eu-N1 (°)		N2-Eu-N2(°)	N1-Eu-N2 (°)	
	50.236×4	91.273×4	63.822×4	63.702×4
	73.249	177.454×2	113.937×4	114.040×4
	74.315	$90.919 \times 2 / 89.024 \times 2$	143.375×2	142.842×2
N1-Ti-N2 (°)		Eu-N1-Ti (°)	Eu-N2-Ti (°)	N1-Ti-N1(°)

	110.172×2	73.014×2	180	84.073×4
	107.426×2	70.801×2		$145.148 / 139.657$
PM	Eu-N1 (Å)	Eu-N2 (Å)	Ti-N1 (Å)	Ti-N2 (Å)
	2.553×2	2.583×4	2.061×2	2.002
	3.779×2	2.277	2.006×2	
	N1-Eu-N1 (°)	N2-Eu-N2(°)	N1-Eu-N2 (°)	
	49.188×4	88.534×4	115.720×4	67.009×4
	64.116	177.067×2	67.612×4	114.857×4
	79.081	$101.928 \times 2 / 77.995 \times 2$	140.460×2	147.942×2
	N1-Ti-N2 (°)	Eu-N1-Ti (°)	Eu-N2-Ti (°)	N1-Ti-N1(°)
	127.947×2	88.407×2	180	89.422×4
	90.940×2	58.882×2		$178.120 / 104.106$

Tetragonal

FM	Eu-N1 (Å)	Eu-N2 (Å)	Ti-N1 (Å)	Ti-N2 (Å)
	3.220×4	$2.731 \times 4 / 2.500 \times 1$	2.039×4	1.855
	N1-Eu-N1 (°)	N2-Eu-N2 (°)	N1-Ti-N1 (°)	N1-Eu-N2 (°)
	50.163×4	89.968×4	84.038×4	113.875×8
	73.667×2	91.364×4	142.398×2	63.715×8
		177.272×2		143.166×4

N1-Ti-N2 (°)		Eu-N1-Ti (°)	Eu-N2-Ti (°)	
108.801×2		71.967×4	180	
AFM	Eu-N1 (Å)	Eu-N2 (Å)	Ti-N1 (Å)	Ti-N2 (Å)
	3.217×4	$2.732 \times 4 / 2.501$	2.041×4	1.855
N1-Eu-N1 (°)		N2-Eu-N2 (°)	N1-Ti-N1 (°)	N1-Eu-N2 (°)
	50.243×4	91.271×4	84.045×4	63.757×8
	73.796×2	89.972×4	142.421×2	113.998×8
			177.458×2	143.102×4
N1-Ti-N2 (°)		Eu-N1-Ti (°)	Eu-N2-Ti (°)	
	108.790×4	71.892×4	180	
PM	Eu-N1 (Å)	Eu-N2 (Å)	Ti-N1 (Å)	Ti-N2 (Å)
	3.172×4	$2.663 \times 4 / 2.278$	1.999×4	1.915
N1-Eu-N1 (°)		N2-Eu-N2 (°)	N1-Ti-N1 (°)	N1-Eu-N2 (°)
	49.647×4	89.298×4	83.556×4	65.800×8
	72.842×2	89.991×4	140.853×2	115.445×8
			178.596×2	143.579×4
N1-Ti-N2 (°)		Eu-N1-Ti (°)	Eu-N2-Ti (°)	
	109.573×2	73.152×4	180	

Table S3. The theoretically calculated lattice parameters, energies and spin moment of the Eu ions (M_{Eu}) of the experimental reported stable Eu^{2+} -containing compounds EuTiO_3 and EuMg_2Sb_2 within different magnetism (PM, FM, A-AFM, C-AFM, and G-AFM denote paramagnetic, ferromagnetic, A-, C- and G-types antiferromagnetic ordering).

Material							
Phase	Magnetism	a (Å)	b (Å)	c (Å)	V (Å 3)	Energy (eV/f.u.)	M_{Eu} (μ_{B})
	(space group)						
	PM	3.8895	/	/	58.843	-29.3538	0
EuTiO_3	FM	3.9051	/	/	59.55	-40.0774	6.959
Cubic	A-AFM	3.9051	/	/	59.55	-40.0765	6.958
$(Pm\bar{3}m)$	C-AFM	3.9051	/	/	59.55	-40.0758	6.957
	G-AFM	3.9051	/	/	59.55	-40.0755	6.954
	PM	5.4347	5.4347	7.8883	232.99	-31.5751	0
EuTiO_3	FM	5.4875	5.4875	7.8714	237.03	-40.1077	6.957
Tetragonal	A-AFM	5.4864	5.4864	7.8666	236.79	-40.1073	6.956
$(I4/mcm)$	C-AFM	5.4883	5.4883	7.8602	236.76	-40.1059	6.955
	G-AFM	5.4866	5.4866	7.8622	236.67	-40.1064	6.952
	PM	4.6646	4.6646	7.3511	138.52	-7.3669	0
EuMg_2Sb_2	FM	4.7009	4.7009	7.6692	146.77	-16.5923	6.981
Trigonal					146.54		
$(P\bar{3}m1)$	A-AFM	4.6950	4.6950	7.6759		-16.5937	6.986

Table S4. The evolution of lattice parameters, separation distances (denoted by d) between the N planes and formation energies (eV/f.u.) of $\text{Ca}_{1-x}\text{A}_x\text{TiN}_2$ ($\text{A} = \text{Sr}, \text{Eu}$) along with ionic substitution content.

	a (Å)	b (Å)	c (Å)	V (Å ³)	b/a ratio	d (Å)	Formation energy
CaTiN_2	3.9512	3.5659	7.5260	106.04	0.90249	0.546	-3.514
$\text{Ca}_{15/16}\text{Sr}_{1/16}\text{TiN}_2$	3.9469	3.5872	7.5388	106.74	0.90887	0.510	-3.529
$\text{Ca}_{14/16}\text{Sr}_{2/16}\text{TiN}_2$	3.9424	3.6085	7.5504	107.41	0.91531	0.473	-3.544
$\text{Ca}_{13/16}\text{Sr}_{3/16}\text{TiN}_2$	3.9416	3.6274	7.5585	108.07	0.92029	0.445	-3.556
$\text{Ca}_{12/16}\text{Sr}_{4/16}\text{TiN}_2$	3.9415	3.6454	7.5662	108.71	0.92488	0.419	-3.569
$\text{Ca}_{8/16}\text{Sr}_{8/16}\text{TiN}_2$	3.9012	3.7566	7.5967	111.33	0.96293	0.204	-3.644
SrTiN_2	3.8936	3.8483	7.6907	115.23	0.98837	0.057	-3.855
CaTiN_2	3.9512	3.5659	7.5260	106.04	0.90249	0.546	-3.514
$\text{Ca}_{15/16}\text{Eu}_{1/16}\text{TiN}_2$	3.9480	3.5821	7.5325	106.53	0.90732	0.520	-3.348
$\text{Ca}_{14/16}\text{Eu}_{2/16}\text{TiN}_2$	3.9496	3.5940	7.5412	107.04	0.90997	0.506	-3.177
$\text{Ca}_{13/16}\text{Eu}_{3/16}\text{TiN}_2$	3.9520	3.6036	7.5425	107.42	0.91184	0.495	-3.004
$\text{Ca}_{12/16}\text{Eu}_{4/16}\text{TiN}_2$	3.9515	3.6195	7.5482	107.96	0.91598	0.471	-2.832
$\text{Ca}_{8/16}\text{Eu}_{8/16}\text{TiN}_2$	3.9526	3.6657	7.5647	109.61	0.92741	0.410	-2.159
EuTiN_2	3.9287	3.7882	7.5988	113.09	0.96424	0.201	-0.848

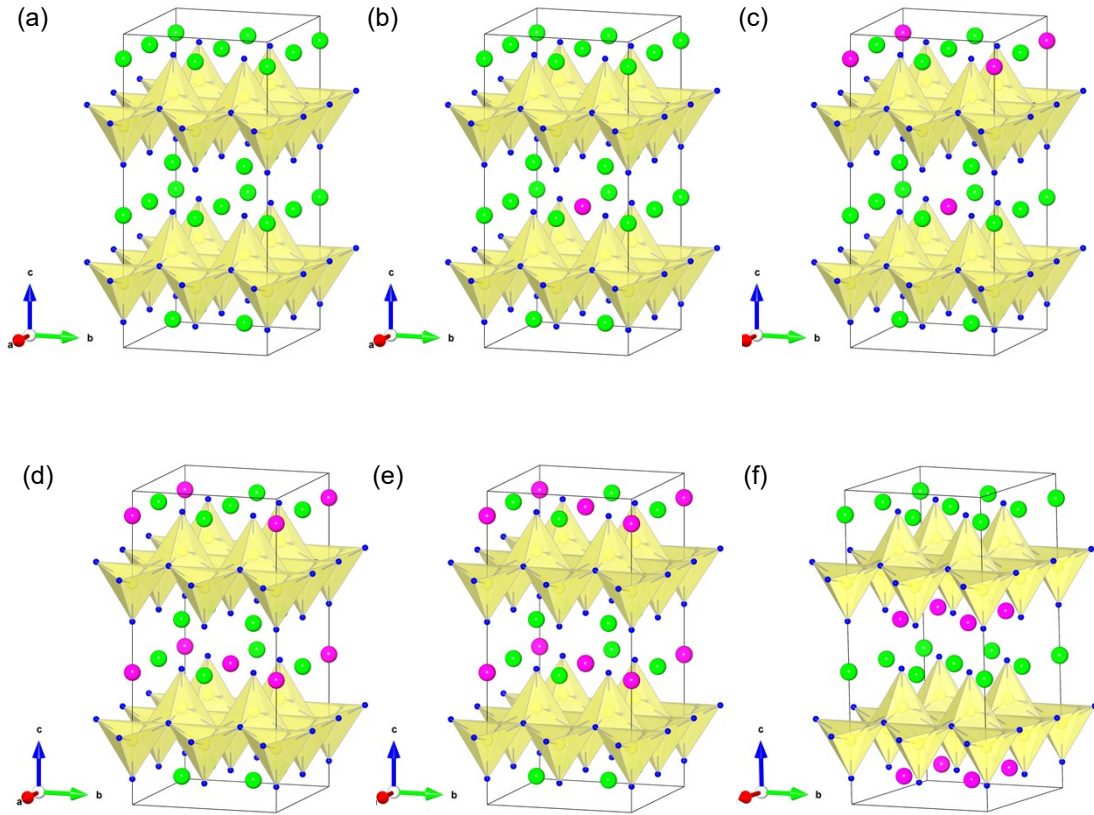


Figure S1. The crystal structure models of the $\text{Ca}_{1-x}\text{A}_x\text{TiN}_2$ ($\text{A} = \text{Sr}$ or Eu) solid solution with compositions of (a) $x = 0$, (b) $x = 0.0625$ (1/16), (c) $x = 0.125$ (2/16), (d) $x = 0.1875$ (3/16), (e) $x = 0.25$ (4/16), and (f) $x = 0.5$ (8/16) within the $2 \times 2 \times 2$ supercells. The big green, big pink and small blue spheres denote the Ca, A and N atoms, while the Ti atoms (yellow spheres) are in the center of the light yellow octahedra.

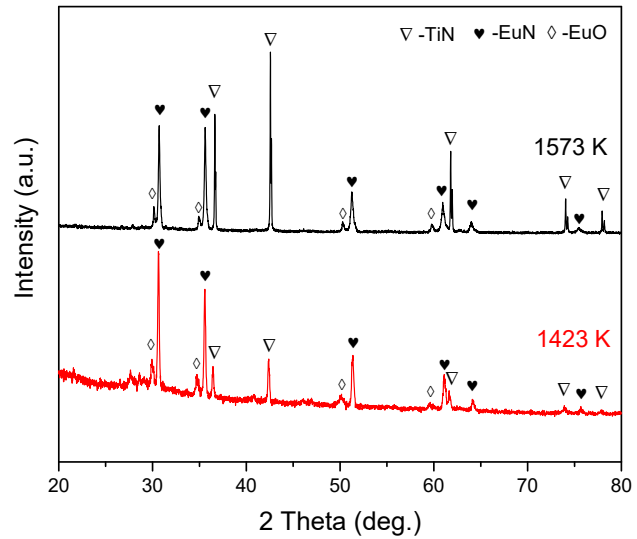


Figure S2. XRD data of nominal EuTiN_2 synthesized at 1573 K and 1423 K.

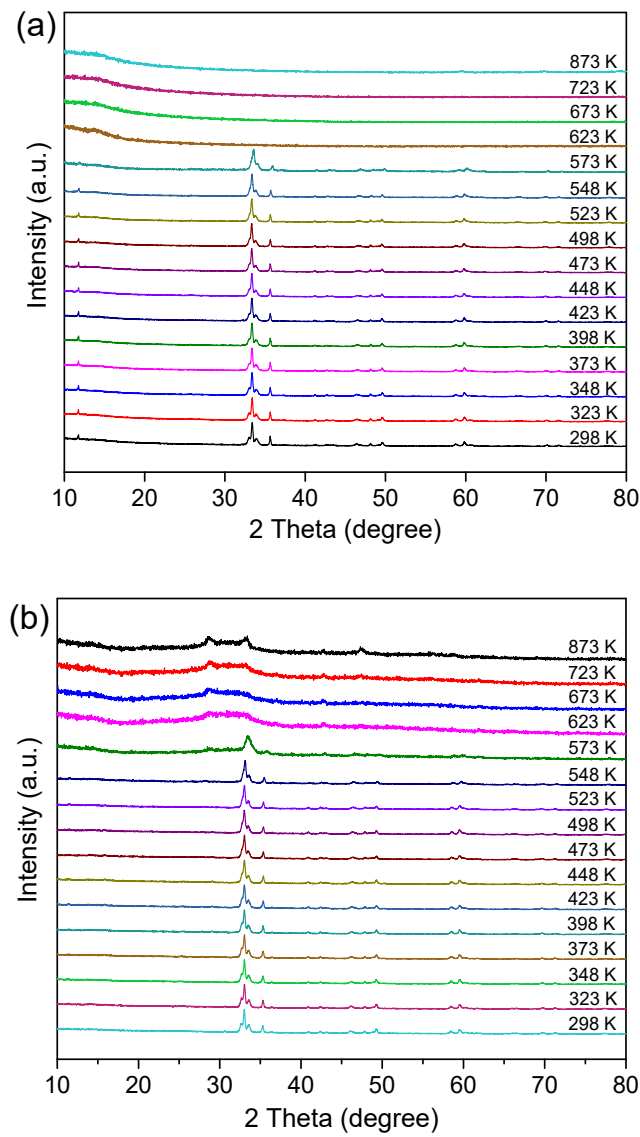


Figure S3. Selected VTXRD data for $\text{Ca}_{1-x}\text{Eu}_x\text{TiN}_2$ solid solutions with (a) $x = 0.25$ and (b) $x = 0.35$.

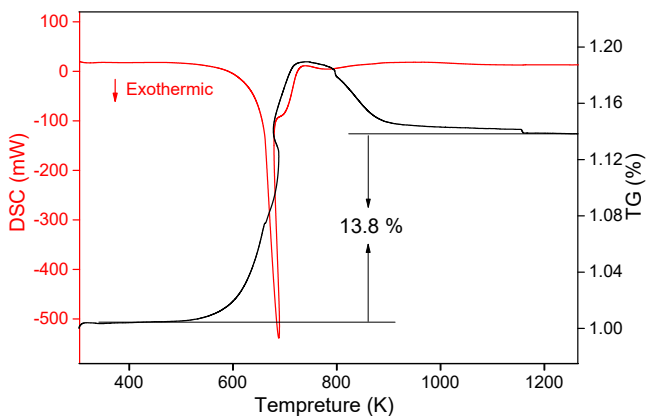


Figure S4. TGA-DSC curve of $\text{Ca}_{0.75}\text{Eu}_{0.25}\text{TiN}_2$ in air atmosphere. The mass gain took place from 500 K and reached a maximum within 700-750 K, followed by a decrease before entering an essentially constant mass region above 900 K. Such TG behavior is common for nitride samples. Since the test was carried out in an air atmosphere, the reaction between the sample and oxygen and other components in air during the heating process could generate some intermediates, which could decompose at high temperature and eventually become stable oxides. Alternatively, as the powder sample was used in the TGA measurement, its surface adsorption may also cause the mass of the sample to increase first and then decrease.^[1, 2]

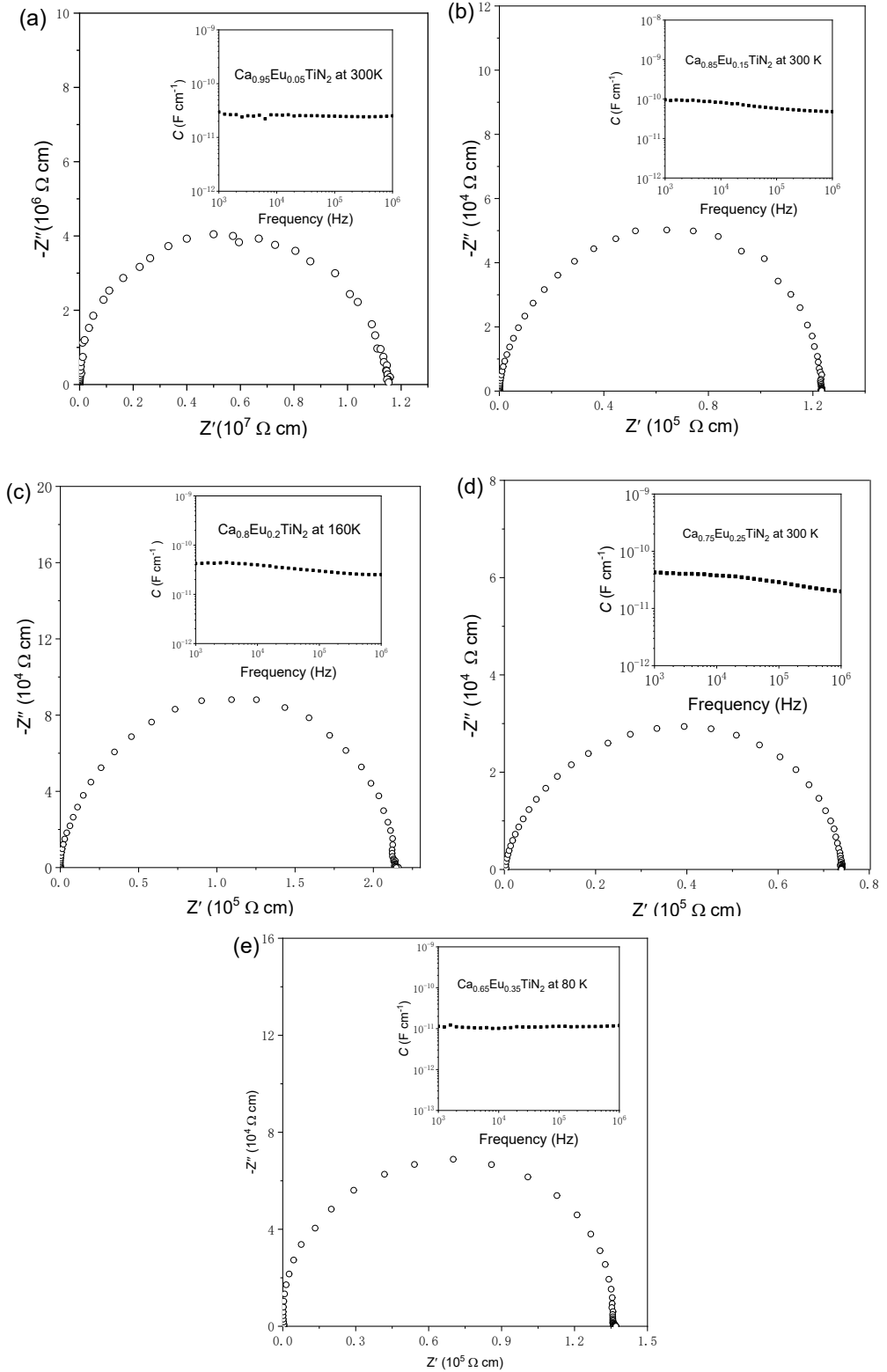


Figure S5. Complex impedance plots of $\text{Ca}_{1-x}\text{Eu}_x\text{TiN}_2$: (a) $x = 0.05$, (b) $x = 0.15$, (c) $x = 0.2$, (d) $x = 0.25$ and (e) $x = 0.35$.

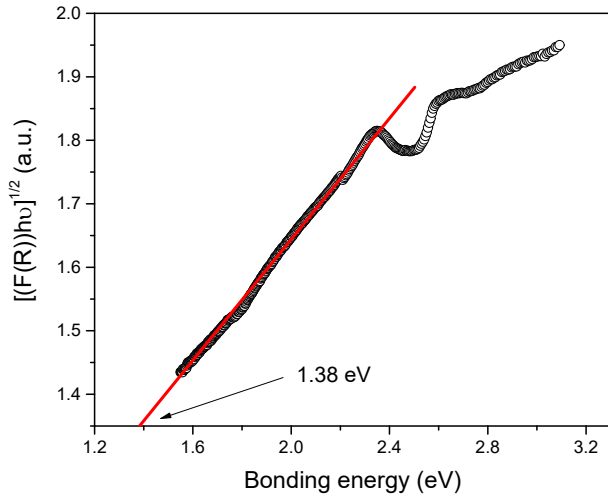


Figure S6. $(\alpha h\nu)^{1/2}$ versus photon energy $h\nu$ plots from the UV-Vis light absorption spectra of $\text{Ca}_{0.8}\text{Eu}_{0.2}\text{TiN}_2$.

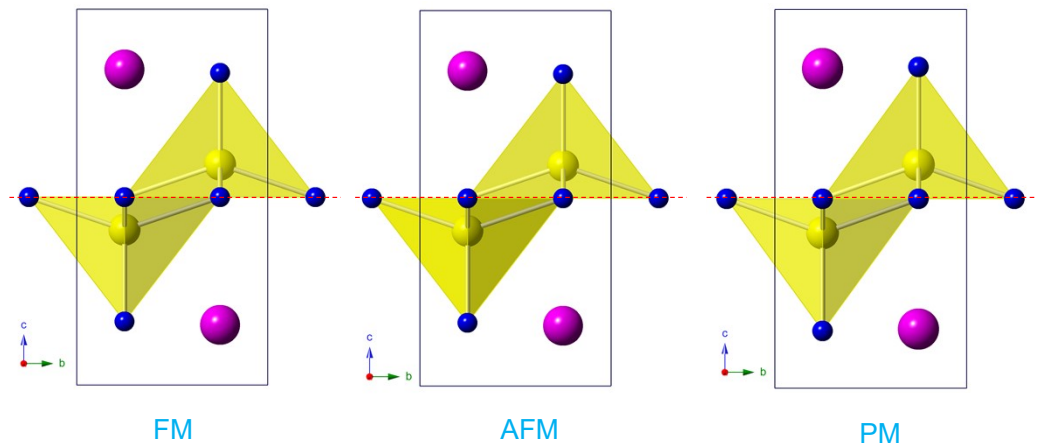


Figure S7. Optimized tetragonal structures of the hypothetical EuTiN_2 in ferromagnetic (FM), antiferromagnetic (AFM) magnetic ordering states and paramagnetic (PM) state. Due to the little difference of the lattice constants, bond lengths and bond angles as tabulated in **Table 1** and **Table S2**, it is hard to visualize the tiny difference between these three structures.

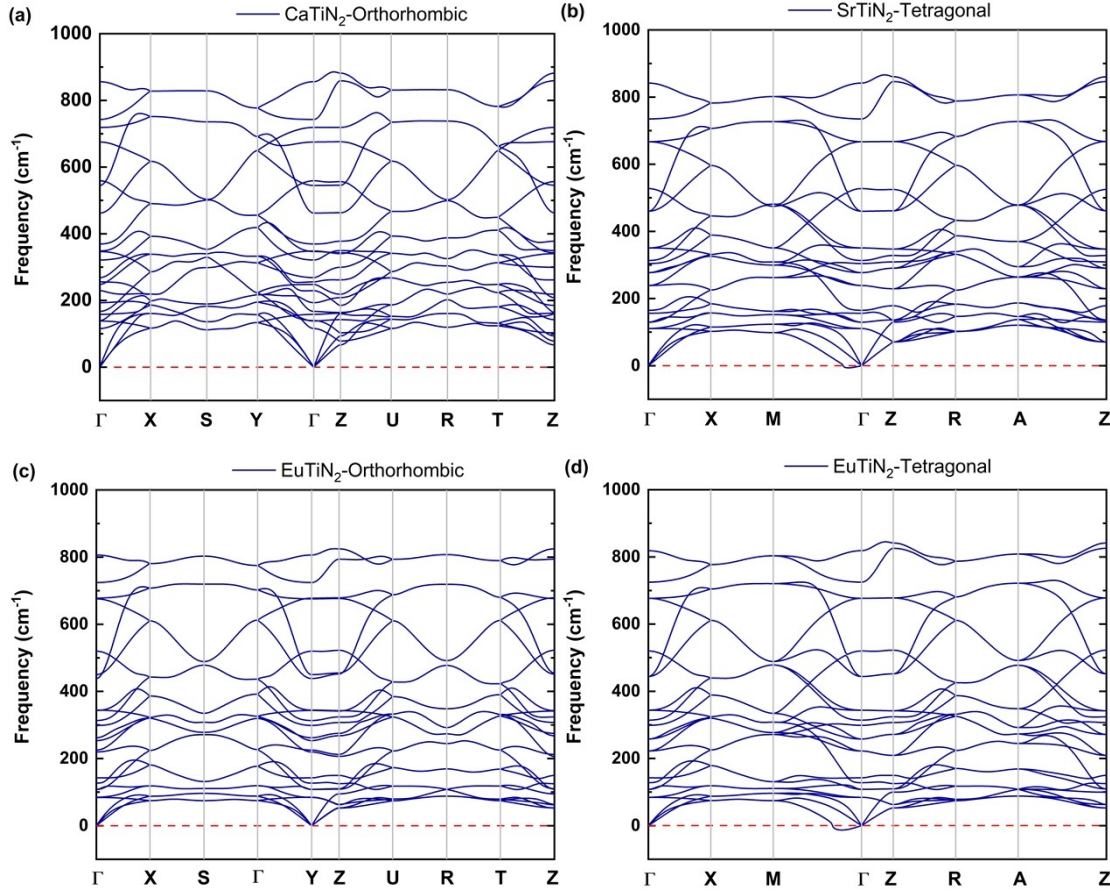


Figure S8. The phonon spectra of the end member of $\text{Ca}_{1-x}\text{A}_x\text{TiN}_2$, *i.e.* ATiN_2 ($\text{A} = \text{Ca}$, Sr , Eu) for the stable orthorhombic and tetragonal phases within a $3\times 3\times 2$ supercell: (a) orthorhombic CaTiN_2 , (b) tetragonal SrTiN_2 , (c) orthorhombic and (d) tetragonal phases EuTiN_2 . The CaTiN_2 and SrTiN_2 were nonmagnetic, whereas the orthorhombic and tetragonal phases EuTiN_2 were calculated for the ferromagnetic (FM) ordering structure. The phonon spectra were calculated using the finite differences method as implemented in VASP. Post-processing and analysis have been performed using the software Phonopy^[3].

Magnetic ordering transition temperature calculations

The magnetic ordering transition temperature T_C (here is the FM Curie temperature) of EuTiN₂ can be estimated according to mean field theory^[4,5], which is

defined as:
$$T_C = \frac{2S(S+1)}{3k_B}(2J_1 + 2J_2)$$
, where k_B is the Boltzmann constant, J_1 and J_2 are the exchange interaction constants between the nearest neighbor and next nearest

neighbor Eu²⁺ ions, S is the spin moment of the Eu²⁺ ion. The exchange constant J_{ij}

describes the interactions between spins S_i and S_j by the classical Heisenberg model:

$$H = -\sum_{i \neq j} J_{ij} S_i \cdot S_j$$
. Due to the structural symmetry, the paths of the J_1 and J_2 exchange interactions are different in the orthorhombic phase, which are the same in the tetragonal phase. Therefore, the exchange constant J_1 (J_2) describes the interactions

between 2 nearest-neighbor (2 next nearest-neighbor) Eu²⁺ ions for the orthorhombic phase due to different Eu-Eu interatomic distances, while there is only one exchange

constant J_1 describes the interaction between 4 nearest-neighbor Eu²⁺ ions for the tetragonal phase due to equal Eu-Eu interatomic distances. In order to derive the

exchange constants, FM and AFM1 configurations are considered for the tetragonal

phase, while FM, AFM2 and AFM3 configurations are considered for the orthorhombic phase, for which the schematic figures are shown in **Figure S9**. By

constructing a 2×2 supercell with two layers of Eu²⁺ ions aligning as depicted in

Figure S9, the total energies per supercell of these magnetic configurations are given

by the equations: $E_{FM} = E_0 - 8J_1S^2 - 8J_2S^2$, $E_{AFM1} = E_0 + 8J_1S^2 + 8J_2S^2$,

$E_{AFM2} = E_0 + 8J_1S^2 - 8J_2S^2$, and $E_{AFM3} = E_0 - 8J_1S^2 + 8J_2S^2$, where S is the spin moment of

the Eu²⁺ ions ($S = 7/2$) and E_0 is the system energy independent of the magnetic

ordering. Then we can deduce the exchange constant $J_1 = \frac{1}{32S^2}(E_{AFM1} - E_{FM})$ for the tetragonal phase, and $J_1 = \frac{1}{16S^2}(E_{AFM2} - E_{FM})$ and $J_2 = \frac{1}{16S^2}(E_{AFM3} - E_{FM})$ for the orthorhombic phase. The exchange constants are obtained as $J_1 = 0.248$ meV and $J_2 = 0.298$ meV for the orthorhombic phase, $J_1 = 0.203$ meV for the tetragonal phase. The Curie temperatures T_c are estimated to be 133 and 99 K for the orthorhombic and tetragonal phases, respectively.

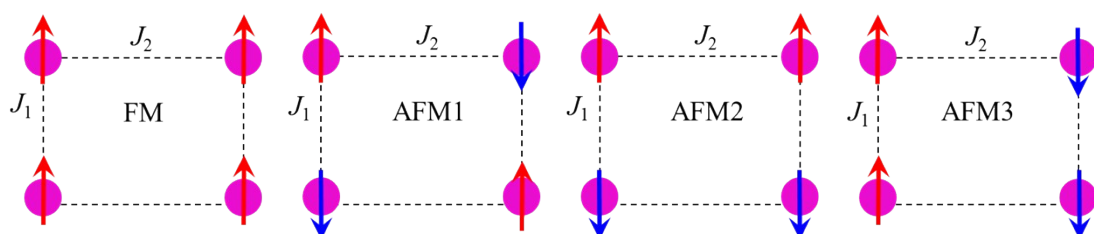


Figure S9. Theoretically hypothetical spin parallel (FM) and spin antiparallel (AFM1, AFM2 and AFM3) configurations of one-layer Eu^{2+} ions in the orthorhombic or tetragonal phase EuTiN_2 . The up/down arrows denote the spin direction of the Eu^{2+} ions. Note that the J_1 and J_2 exchange interactions are the same in the tetragonal phase.

References

- (1) D. Logvinovich, L. Bocher, D. Sheptyakov, et al., Solid State Sci. **2009**, 11, 1513-1519.
- (2) F. Oehler, H.T. Langhammer, S.G. Ebbinghaus J. Eur. Ceram. Soc. **2017**, 37, 2129-2136.
- (3) A. Togo, I. Tanaka, Scripta Mater. **2015**, 108, 1-5.
- (4) P. Kurz, G. Bihlmayer, S. Blugel, J. Phys-Condens. Mat., 2002, 14, 6353-6371.
- (5) Y. Fujioka, J. Frantti, R.M. Nieminen, J. Phys. Chem. B, 2008, 112, 6742-6746.